# Volcanic Origin of a Long-Lived Swarm in the Central Bransfield Basin, Antarctica

P. Poli, L. Cabrera, M. C. Flores, J. C. Báez, J. B. Ammirati, J. Vásquez, S. Ruiz

AGU ADVANCING EARTH AND SPACE SCIENCE

Geophysical Research Letters®

RESEARCH LETTER
10.1029/2021GL095447

**Key Points:**

- We characterized one of the largest swarms ever recorded in a spreading ridge
- Analysis of seismological and geodetic data suggest volcanic origin for this swarm
- We infer a significant role played by axial volcanic structures in opening of spreading ridges

**Supporting Information:**

Supporting Information may be found in the online version of this article.

**Correspondence to:**

P. Poli,
pieropoli85@gmail.com

**Citation:**

Poli, P., Cabrera, L., Flores, M. C., Báez, J. C., Ammirati, J. B., Vásquez, J., & Ruiz, S. (2022). Volcanic origin of a long-lived swarm in the central Bransfield Basin, Antarctica. *Geophysical Research Letters*, *49*, e2021GL095447. https://doi.org/10.1029/2021GL095447

Received 30 JUL 2021
Accepted 17 DEC 2021



# Volcanic Origin of a Long-Lived Swarm in the Central Bransfield Basin, Antarctica

**P. Poli[1], L. Cabrera[1], M. C. Flores[2], J. C. Báez[2], J. B. Ammirati[3], J. Vásquez[4], and S. Ruiz[5]**

[1]ISTerre Institut des Sciences de la Terre, CNRS, Université Grenoble Alpes, Grenoble, France, [2]Centro Sismológico Nacional, Universidad de Chile, Santiago, Chile, [3]Department of Geology, Faculty of Physics and Mathematics, Universidad de Chile, Santiago, Chile, [4]Facultad de Ciencias de la Salud, Universidad de Talca, Talca, Chile, [5]Department of Geophysics, Faculty of Physics and Mathematics, Universidad de Chile, Santiago, Chile

**Abstract** Understanding the extensional processes in tectonic context at the transition from continental to oceanic spreading is fundamental to obtain new insights about formations of new oceans. To that scope, we study a large and long-lived earthquake swarm occurring in 2020–2021 in a back-arc rift (the Bransfield Basin) south of the South Shetland Islands, Antarctica. We make use of one local seismological station to detect more than 36,000 small earthquakes, occurring from August 2020 to June 2021. Together with the occurrence of earthquakes, we observe a significant, geodetic deformation at a nearby GPS station. By joint interpretation of b-value, spatiotemporal evolution of seismicity and geodetic deformation, we infer a volcanic origin for this swarm that takes place close to the ridge axis. Our study suggests that beyond the 7 mm/yr deformation reported at the Bransfield Basin ridge, transient deformation episodes localized at the ridge axial volcanic structure also modulate the extension.

**Plain Language Summary** Understanding the extensional tectonics in places at the transition from continental to oceanic spreading, can provide new insights about the extensional processes leading to formation of new oceans. We report on a long-lived (∼1 year) earthquake swarm in the Bransfield Basin, just south of the South Shetland islands, in Antarctica, that brings new observations to such tectonics. This basin represents a ridge separating two tectonic plates and is characterized by extensional tectonics at the transition from back-arc rifting to ocean spreading. By detection and characterization of more than 36,000 earthquakes and observation of associated geodetic deformation, we inferred the significant role played by volcanic processes occurring at the ridge axis, in modulating extension of the basin. This observation differs from models of purely tectonic extensional processes involving rift bounding border faults.

## 1. Introduction

In August 2020, a significant increase of seismic activity was reported in the Bransfield Basin, south of the South Shetland islands, Antarctica (Figure 1). Between 29 August 2020 and June 2021, the United State Geological Survey (USGS, 2020) reported 128 earthquakes with magnitudes larger than 4.0 (Figure 1). The seismicity was not characterized by any large mainshock (Figure S1 in Supporting Information S1) that could potentially have triggered the prolific occurrence of earthquakes in the region. Similar observations were recently reported by Olivet et al., (2021).

The central Bransfield Basin is a ridge separating the Antarctic plate to the South, from the South Shetland microplate (Almendros et al., 2020; Olivet et al., 2021; Taylor et al., 2008 and reference therein, Figure 1). The NW-SE extension of the ridge results from the combination of slab rollback from the past subduction of the Phoenix microplate under the South Shetland microplate, and transtensional motion between the Scotia and Antarctic plates (Almendros et al., 2020; Gràcia et al., 1996; Taylor et al., 2008). The basin is also characterized by extensive volcanism (Almendros et al., 2020; Taylor et al., 2008), occurring in several submarine structures, such as the Orca volcano, that is located ∼20 km southwest of the seismic swarm (Figure 1, Almendros et al., 2020; Olivet et al., 2021). The Orca Volcano consists of a large caldera surrounded by shallow magma reservoirs (Almendros et al., 2020). The Orca volcano magmatism is mostly basaltic with mid-ocean ridge characteristics (Barker & Austin, 1998) and significant hydrothermal activity is also observed in the area (Bohrmann et al., 1998). The volcano's caldera and shallow magmatic bodies produce a positive magnetic anomaly extending along the axis ridge (Almendros et al., 2020). The 2020–2021 swarm overlaps with the shallow magnetic anomaly located northeast

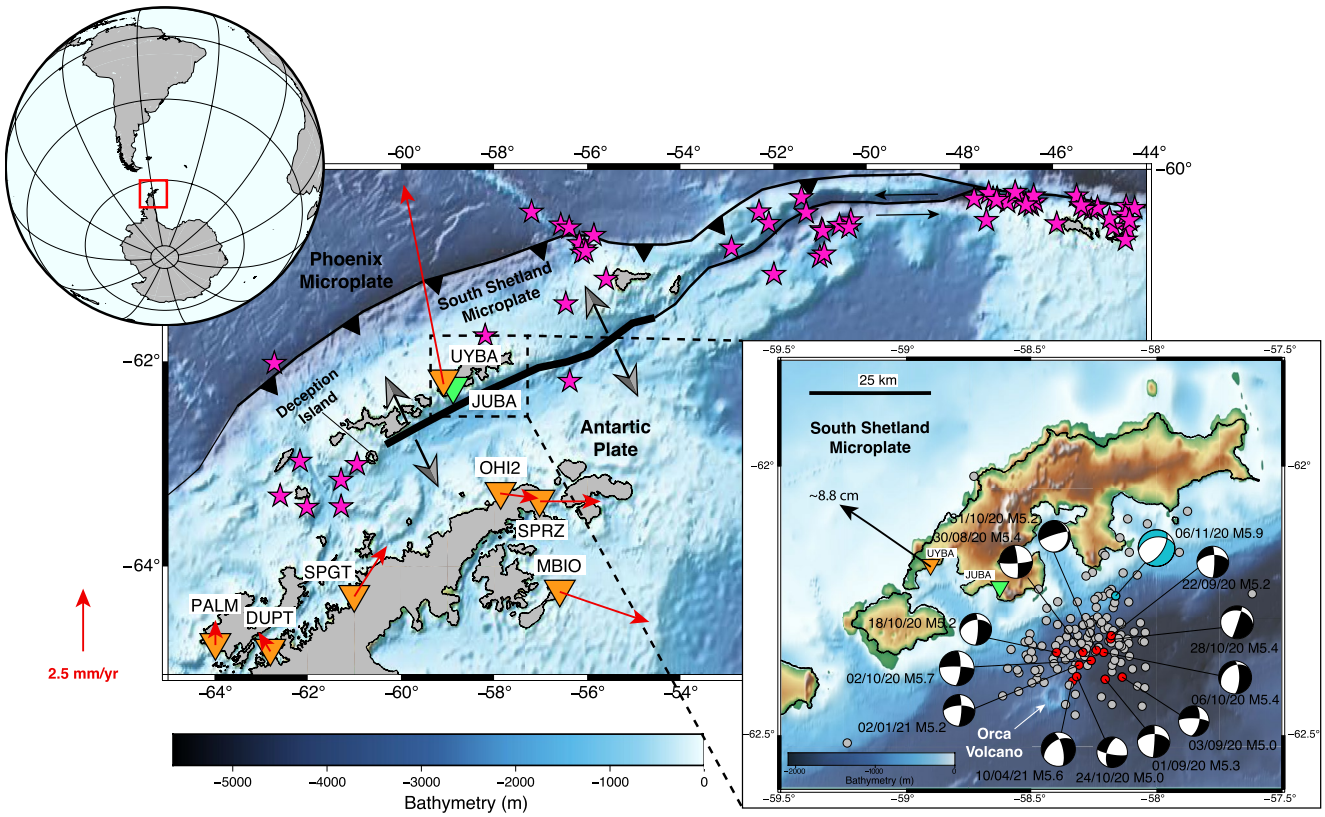


**Figure 1.** Orange inverted triangles indicate GNSS stations and the green inverted triangle shows the location of the JUBA broad-band station. Pink stars represent historical seismicity with magnitudes equal or larger than 5.5 from the ISC (International Seismological Centre, 2021) occurred after the eruption of Deception Island (12 August 1970). Red arrows represent velocities of the stations (see text for details about GPS processing). Right inset: Focal mechanisms (colored compressional quadrants) reported by the USGS since 28 August 2020 and the location of the Orca volcano. Date dd/mm and magnitude are also indicated. The cyan focal mechanism is for the largest event (Mw5.9) also indicated in Figures 4 and S4 in Supporting Information S1. The estimated NW displacement for UYBA with respect to the Antarctic plate is indicated with a black arrow (see text for details about GNSS processing).

of the Orca volcano (Almendros et al., 2020; Olivet et al., 2021). Several other swarms connected with volcanic activity have also been observed along the Bransfield Ridge (Almendros et al., 2018; Dziak et al., 2010), but are mostly located in the western part of the ridge. No significant earthquakes have occurred in the central Bransfield basin since 1970 (Figure 1).

The Bransfield Ridge is of major geological interest as it represents a back-arc basin at the transition from rifting to ocean spreading (Almendros et al., 2020). Detailed analysis of the 2020–2021 earthquake sequence therefore provides new insights about short term processes associated with the evolution from rifting to spreading, and attempts to distinguish if this swarm, and the related geodetic deformation, is the result of extensional tectonics or volcanic process (Bergman & Solomon, 1990; Buck, 2004; Reiss et al., 2021). To address this question, we make use of the limited, but significant data available from the region (Figure 1). One seismic station (JUBA, network AI) located at the Carlini Base (King George Island, ~20 km from the swarm, Figure 1) is used to improve the detection of earthquakes using template matching (Gibbons & Ringdal, 2006) and to characterize the waveforms associated which each detected event. We also analyzed data from the nearby GNSS stations (Figure 1), to assess any deformation associated with the seismic activity. Despite the limited data available, we were able to characterize the early phase and development of the largest swarm ever observed in the Bransfield Ridge area. Our observations to support the hypothesis of a volcanic origin of this earthquake sequence.

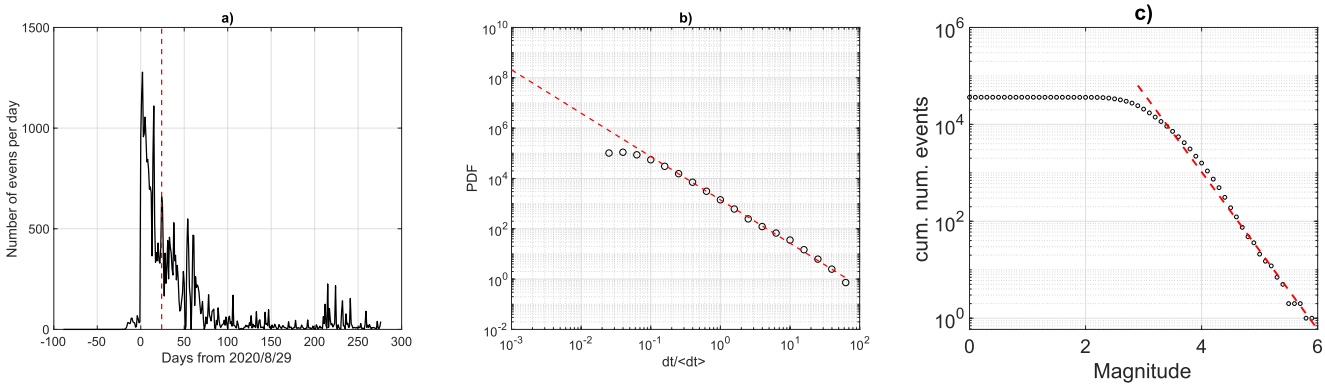


**Figure 2.** (a) Number of events as function time with respect to 8 August 2020, with the vertical red dashed line highlighting the occurrence of the largest event in the sequence. (b) Distribution of inter-event waiting time (dt) for the detected events. The red line shows the fit of this data with Equation 1 and $\gamma = 0.6$. (c) Cumulative magnitude-frequency distribution for the detected earthquakes. The red dashed line shows the regression for magnitudes ranging from 3 to 6. The corresponding b-value is 1.6.

## 2. Data and Methodology

### 2.1. Earthquakes Detection and Characterization

We use a seismic station located ∼20 km NW from the swarm centroid (Figure 1) to systematically detect and characterize seismic events in the study area. We first downloaded 1 year (1 June 2020, to 1 June 2021) of continuous three-component waveforms recorded at station JUBA (Istituto Nazionale di Oceanografia e di Geofisica Sperimentale, 1992) at 100 Hz sampling rate. The traces are first band-pass filtered between 1 and 9 Hz to enhance high frequency signals from the local seismicity and resampled at 50 Hz. Then, we extracted the events corresponding to the USGS catalog (Figure 1) within a 12s window (starting 2 s before *P*-wave arrival), ensuring the presence of both P- and S-waves associated with the swarm events. We visually controlled the quality of each seismogram and manually picked the *P*- and *S*-waves on good quality seismograms exhibiting phases well identifiable on the three components. This process yielded 114 earthquakes, the waveforms of which represent the templates to scan the continuous data. We then performed the detection of new events with template matching (Gibbons & Ringdal, 2006) and a single station approach (Bell et al., 2021; Poli, 2017; Van der Elst et al., 2013). Because the use of a single station can reduce the detection sensitivity and increase the presence of unwanted signals, we combined visual inspection and detection with fake templates (e.g., waveforms flipped in time, Cabrera et al., 2020), to define an optimal detection threshold (3-components average correlation coefficient greater than 0.5). The correlation threshold was set after an extensive visual inspection of the detected waveforms, to exclude false events from our final catalog. At this stage several detections can results from multiple templates over the time window of a template (12 s). To remove multiple detections, we keep the event with the largest correlation coefficient as the final detection.

The template matching identified 36,241 earthquakes, ∼300 times more than the initial catalog (Figure 1). Figure S2 in Supporting Information S1 shows examples of detected waveforms.

We estimated the magnitude of each newly detected event by computing the mean *S*-wave amplitude ratio between the template events and our detections over the three components. Using the template event's catalog magnitude as a reference, the detection magnitude can then be determined assuming a ratio of 10 corresponds to a variation of one-unit magnitude (e.g., Kato et al., 2016; Sanchez-Reyez et al., 2021). The average mean error between the estimated magnitudes and the USGS ones for our template is 0.2.

Figure 2a shows the temporal variations of the seismicity rate. Unlike what can be observed from the initial catalog, in which the first event occurs on 29 August 2020, the swarm begins on 7 August 2020, with an acceleration leading to the 1,200 events/day recorded on August 29th (Figure 2a). The rate of seismicity then decreases with a log-like behavior similar to an Omori law (Omori, 1894), as is often observed for aftershock sequences although no mainshock was observed at the beginning of the sequence. Indeed, the largest event ($M = 5.9$) occurred on 6 November 2020 (Figure S1 in Supporting Information S1). After this event, the seismicity dropped rapidly (Figures 2 and S1 in Supporting Information S1).

We study in more detail the time evolution of the sequence by calculating the distribution of waiting time ($dt$) in between events (e.g., Duverger et al., 2018, Figure 2b). We fit the waiting time with a gamma distribution:

$$\rho(dt) = A\left(\frac{dt}{\langle dt\rangle}\right)^{\gamma-1} exp\left(\frac{-dt}{\langle dt\rangle}\right) \quad (1)$$

where $A$ is a constant (Hainzl et al., 2006). The fitting results provides $\gamma = 0.6$, a value which differs from mainshock-aftershocks style of seismicity ($\gamma_{aftershocks} = 0$). Our result implies a clustered seismicity, but little interaction in between events (Duverger et al., 2018; Hainzl et al., 2006). We can thus rule out static and dynamic events interaction as a driver for this sequence (e.g., events triggered by mainshocks), as discussed in previous works (Duverger et al., 2018; Hainzl et al., 2006). The seismicity must therefore be driven by an external forcing (e.g., Bourouis & Bernard, 2007; Duverger et al., 2018; Hainzl et al., 2006; Perfettini & Avouac, 2004) likely to be a magmatic process occurring in the ridge. Similar observations (no clear mainshock, slow decay of the seismicity) were observed for the 2014–2015 Deception Island volcanic swarm, in the western part of the Bransfield Basin (Almendros et al., 2018).

To gain more insights about the possible origins of this swarm we also assessed the b-value (Gutenberg & Richter, 1941). For regular earthquake sequence, b-value is usually around 1 (Frohlich & Davis, 1993), and deviation from this average can provide information about stress and/or physical properties of the rock volume (Farrell et al., 2009; Mogi, 1962; Schorlemmer et al., 2005). We use the magnitude frequency distribution of Figure 2c to estimate a b-value of $1.6 \pm 0.1$, using a least squares method and considering a magnitude completeness of 2.9, estimated from maximum curvature method (Wiemer, 2001). We further study how the errors in magnitude estimation affect the estimation of the b-value, by simulating 1,000 catalogs with randomly perturbed magnitude up to 0.2 magnitude units. With this approach, we obtained a final average b-value of 1.6 with standard deviation of 0.06.

The estimated b-value is remarkably higher respect with values characterizing regular earthquake sequences (Farrell et al., 2009; Frohlich & Davis, 1993). It is also remarkably different than previous studies in this area (Olivet et al., 2021), which found a b-value of ∼1.2. Our detection of events with much smaller magnitudes allowed us to better resolve the b-value for this swarm. Such a high b-value coincides with other values observed in volcanic areas (e.g., Farrell et al., 2009; Roberts et al., 2015; Wilks et al., 2017).

No clear spatial migration of the seismicity can be observed from the USGS earthquake locations (Figure S3 in Supporting Information S1). However, teleseismic events are usually characterized by significant uncertainties, which could bias this kind of observation. While we could not locate the microseismic events detected, due to small events being visible only at JUBA (Figure 1), we attempted to discern any spatiotemporal patterns from S-P time analysis, using a single station approach. We first analyzed if any general migration was visible, by plotting the S-P time picked at station JUBA (Figure 1) when selecting templates (Figure 3a). No clear global spatial migration was observed but rather some time-limited migration episodes and a shift of the seismicity farther from JUBA starting mid-October 2020 (Figure 3a). Despite the scarce information about the velocity structure in the area, we can get some insights about the extent of the swarm from the S-P time. We assume a Vp = 6 km/s and Vp/Vs = $\sqrt{3}$. Using the mentioned Vp and Vs the spatial difference for the average S-P time of 2.6s is ∼21 km.

We also evaluated the relative *P*- and *S*-wave travel times for all events detected by a single template (a family of events). For some of the biggest families we used the templates as reference waveforms, and estimated the delay with respect to the reference events, by cross correlating 1 s of signal around P and S arrivals. For this analysis, the original sampling rate (100 Hz) at JUBA station was used.

Figures 3b and 3c shows the results for the two largest families, for P and S delays with correlation coefficients larger than 0.7. The seismicity is clustered within a small area, similar to previous volcanic swarms observed in this region (Almendros et al., 2018, Figure 3). The time delays show short times of coherent delays associated with bursts of seismic events. A possible diffuse migration toward the station can be observed at the beginning of the sequence (Figure 3b). From the analysis of the delay time, we also observed migration of the seismicity farther from JUBA station (Figure 3c), in late October and early November 2020, also inferred from S-P time differences (Figure 3a).

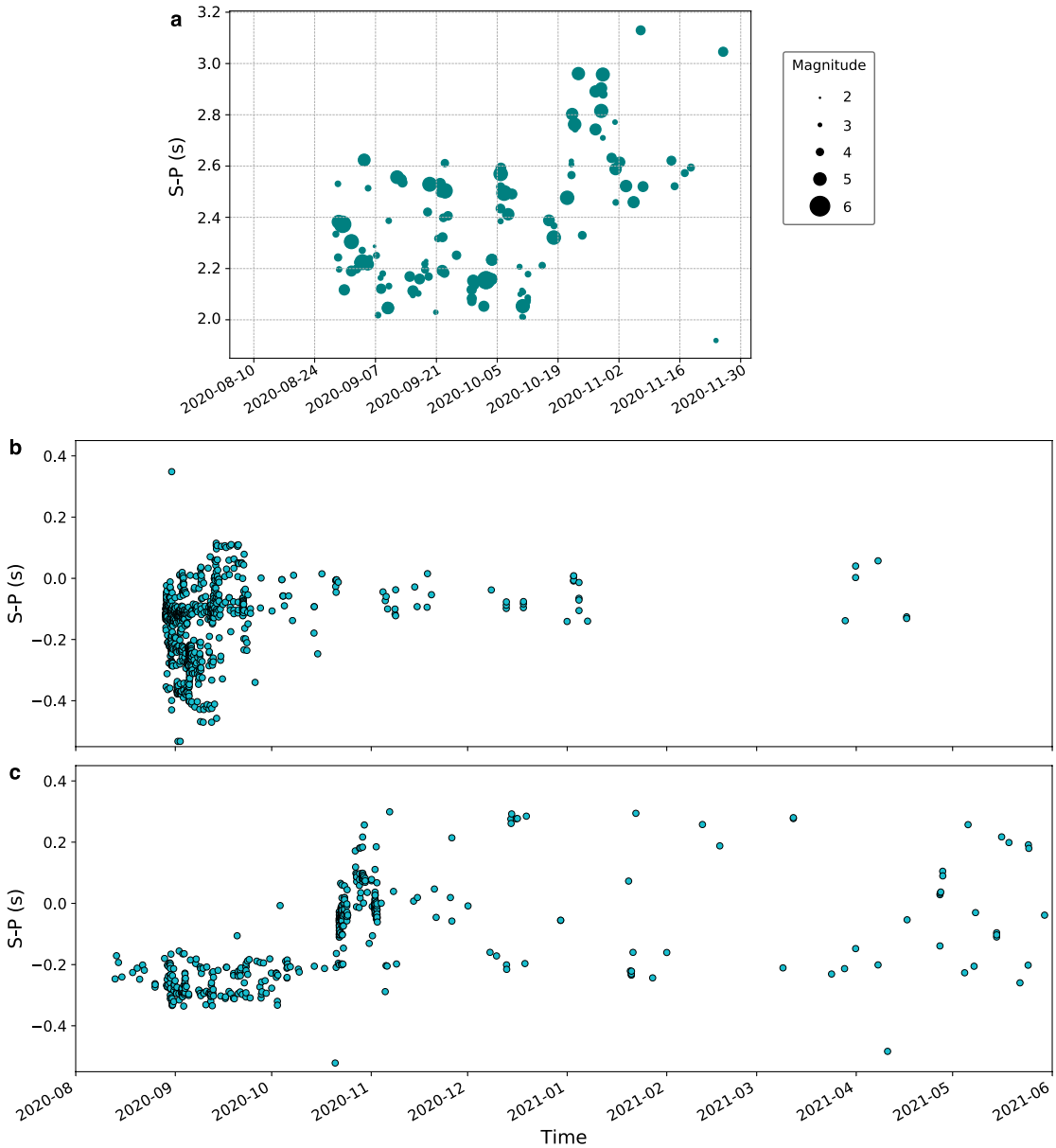


**Figure 3.** S-P time from manual picking performed on 114 templates (a) and from delay estimated from cross-correlation of earthquakes detected (b–c).

### 2.2. Geodetic Observations

We use GNSS observations from 2017 to June 2021, from a set of stations located around the area (Figure 1). All observations were processed in a network array including several IGS regional stations, applying the differential approach strategy with the Bernese GNSS Software V5.2 (Báez et al., 2018). We stack all daily solutions to generate time series of deformation with respect to the Antarctic plate (Figure 4). More details about processing of GNSS data can be found in Supporting Information S1, together with the estimated velocities (Table S1 and Figures S4, S5 in Supporting Information S1).

The detrended GNSS time series located on the northern zone of Antarctica (UYBA, OHI2, MBIO and SPRZ) show residual deformation consistent with extensional process prior to 29 August 2020 (Figures 4a and 4b). However, no GNSS time series show a clear increase of velocity during the seismicity rate acceleration between 7 and 28 August 2020 (Figures 2a, 3c–3e). The most important velocity change with a clear centimetric displacement (Figures 1 and 4) is observed from August 28th to June 2021 (when our analysis ends) on both the north and east

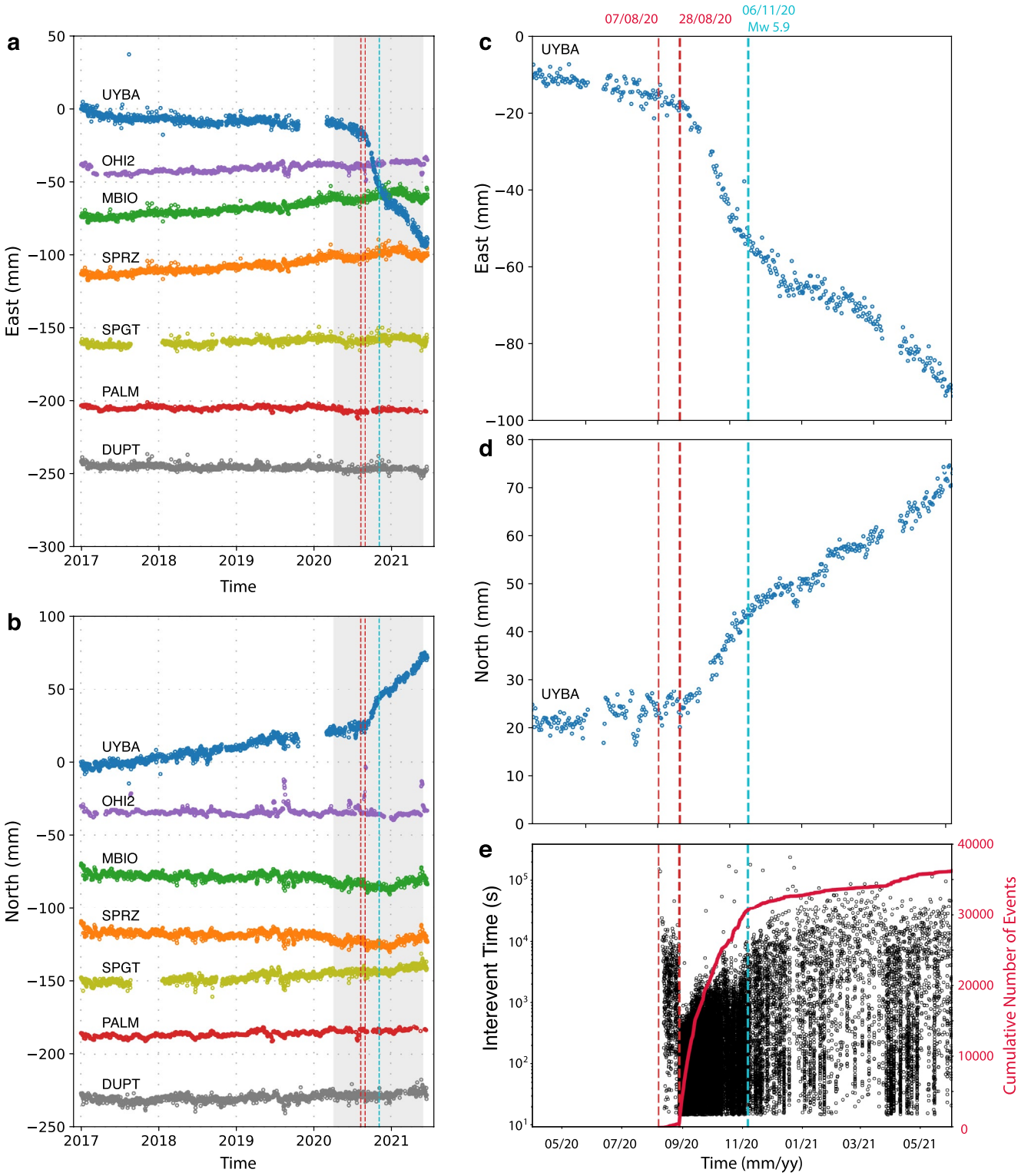


**Figure 4.** GPS displacement at stations reported in Figure 1 for the east (a) and north (b) components. (c and d) are zooms during the swarm time for station UYBA (see Figure 1). (e) Cumulative number of events as function of time in red, and recurrence time of events in black dots.

components of station UYBA. The displacement vector is orthogonal to the Bransfield rift axis and is consistent with previous observations from the interseismic period (Taylor et al., 2008). This relative geometry agrees with rift opening dynamics (Almendros et al., 2020; Taylor et al., 2008). The evolution of GNSS displacement at station UYBA during the swarm (Figures 4c and 4d), closely follows the log-like decrease in cumulative events (Figure 3) for the first part of the sequence, suggesting that both seismicity and surface displacements are driven by the same process (either slow tectonic deformation or volcanic activity). In addition, after the occurrence of a Mw5.9 event on 6 November 2020, we further observe that the seismicity rate starts to decay along with GNSS velocities (Figure 3).

## 3. Discussion and Conclusions

Despite a scarce geophysical instrumentation, we were able to document and characterize the largest earthquake swarm ever recorded in the Bransfield Basin (Almendros et al., 2018; Dziak et al., 2010). We detected a long-lived swarm of more than 36,000 earthquakes that began on 7 August 2020, and accelerated on 29 August 2020, challenging previous findings from Olivet et al. (2021). The seismicity rate decreases following a log-like behavior, although no mainshock was observed at the beginning of the swarm (Figure 2). The detailed analysis of recurrence time (Figure 2b) allows us to rule out the mainshock-aftershock mechanism as the mechanism driving the occurrence of the large number of recorded events, and observed GNSS deformation (Figure 4). The cumulative number of earthquakes closely follows the deformation observed at the GNSS station on King George Island (Figures 1 and 4). Despite the noise in GNSS time series (Figures S6–S13 in Supporting Information S1), probable from response to ice load changes, the orientation of the deformation is orthogonal to the ridge (Figure 1) and suggests that the ridge spreading is responsible for the 8 cm displacement (Figures 1 and 4). The deformation on King George Island could occur either in response to a dike intrusion (Heimisson & Segall, 2020) or could be associated with a large slow slip event with extensional geometry.

As previously mentioned, the increase in seismicity rate was not preceded by any clear mainshock (Figure S1) and shows a very slow decay in time (Figures 2a and 2b). Both observations suggest a swarm-like sequence (Mogi, 1963), with limited interaction in between events (Figure 2b). This swarm is thus likely to be driven by external forcing, also responsible for the deformation observed in the GNSS data (Figure 4). The estimated b-value is ∼1.6, a significantly larger value than previous estimates based on a smaller seismicity catalog (Olivet et al., 2021). We suggest that this difference arises mainly from our improved detection of events with template matching (36,241 events), which permits to outpace the number of events detected from a visual inspection approach, made by Olivet et al. (2021) (3,186 events). This large b-value can result from stress heterogeneity, significant thermal gradient and/or presence of magmatic fluids which has been observed in volcanic areas (Farrell et al., 2009). Beyond reporting a different b-value and more events than Olivet et al., (2021) we also better characterize their time evolution (Figures 2a and 2b) and compare it with GNSS deformation recorded during the seismic activity (Figure 4) which allows us to better support our conclusions.

The spatiotemporal analysis of the seismicity (Figure 3) resolved with a single station approach, reveals that the swarm nucleated on a small region, with rapid migrations and quick activation of small seismic bursts (Figure 3). No clear large-scale spatially coherent migration of the seismicity, as the one related to dyke injection discussed by Roman and Cashman (2006), is observed. This behavior can reflect a strong stress heterogeneity (Farrell et al., 2009) also suggested by the high b-value (Figure 2). We further observe that seismicity mostly lies in a region of high positive magnetic anomaly (Almendros et al., 2020), interpreted as a shallow magmatic body. In addition, most of the large events show strike-slip mechanisms, similar to the swarm model of Hill (1977) and Roman and Cashman (2006). The relatively small number of extensional earthquakes (Figure 1) suggests that deformation related to rifting (Reiss et al., 2021) is limited during this 2020–2021 long episode.

Taken together, our observations suggest a volcanic origin for the 2020–2021 Bransfield Ridge deformation episode (Bergman & Solomon, 1990). We cannot however further discuss the detailed processes occurring during this swarm given the limited amount of data available in the region. We propose that the driving mechanism of the deformation can be either hydrothermal fluids (Reiss et al., 2021) or magma flows (e.g., shallow dike propagation Heimisson & Segall, 2020) at crustal level favored by the presence of conjugate faults (Hill, 1977). The seismicity can also result from local increment of pore fluid pressure (Sibson, 2000). This long-lasting volcanic activity is responsible for the significant deformation inferred from GNSS observations, while seismicity is a by-product of

the magmatic activity (Heimisson & Segall, 2020), mainly occurring in limited areas with brittle characteristics and accumulation of stress (Hill, 1977). Our study also illustrates that, beyond the continuous 7 mm/yr extension (Taylor et al., 2008) between the Antarctica Plate and the South Shetland microplate, rapid deformation episodes occurring at the ridge axial volcanic structures plays a main role in modulating the long-term extension. Finally, our study highlights the main role of magmatic structures in favoring the rifting process instead of tectonic deformation occurring in rifting bounding border faults (Buck, 2004; Reiss et al., 2021).

## Data Availability Statement

Seismological data are available through the IRIS Data Management Center (IRISDMC) at http://service.iris.edu/fdsnws/dataselect/1/ and can be obtained using the **IRIS DMC FDSNWS web service**. The corrected GPS time series are at https://www.csn.uchile.cl/red-sismologica-nacional/red-gps/.

**Acknowledgments**
PP and LC received funding from the European Research Council (ERC) under the European Union Horizon 2020 Research and Innovation Programme (grant agreements, 802777-MONI-FAULTS). JCB was also supported by ANID PIA (ACT192169). SR and JCB were supported by Fondecyt project (N° 1200779, ANID, Chile). JBA is supported by Fondecyt project (N° 3200633, ANID, Chile). SR thanks to Programa de Riesgo Sísmico (PRS) from University of Chile, Chile.

## References

Almendros, J., Carmona, E., Jiménez, V., Díaz-Moreno, A., & Lorenzo, F. (2018). Volcano-tectonic activity at deception island volcano following a seismic swarm in the Bransfield Rift (2014–2015). *Geophysical Research Letters*, *45*(10), 4788–4798. https://doi.org/10.1029/2018gl077490

Almendros, J., Wilcock, W., Soule, D., Teixidó, T., Vizcaíno, L., Ardanaz, O., et al. (2020). BRAVOSEIS: Geophysical investigation of rifting and volcanism in the Bransfield strait, Antarctica. *Journal of South American Earth Sciences*, *104*, 102834. https://doi.org/10.1016/j.jsames.2020.102834

Báez, J. C., Leyton, F., Troncoso, C., del-Campo, F., Bevis, M., Vigny, C., et al. (2018). The Chilean GNSS network: Current status and progress towards early warning applications. *Seismological Research Letters*, *89*, 1546–1554. https://doi.org/10.1785/0220180011

Barker, D. H. N., & Austin, J. A., Jr. (1998). Rift propagation, detachment faulting, and associated magmatism in Bransfield Strait, Antarctic Peninsula. *Journal of Geophysical Research*, *103*(B10), 24017–24043. https://doi.org/10.1029/98jb01117

Bell, A. F., Hernandez, S., Mccloskey, J., Ruiz, M., Lafemina, P. C., Bean, C. J., et al. (2021). Dynamic earthquake triggering response tracks evolving unrest at Sierra Negra volcano, Galápagos Islands. *Science Advances*, *7*(39), eabh0894. https://doi.org/10.1126/sciadv.abh0894

Bergman, E. A., & Solomon, S. C. (1990). Earthquake swarms on the mid-Atlantic Ridge: Products of magmatism or extensional tectonics? *Journal of Geophysical Research*, *95*(B4), 4943–4965. https://doi.org/10.1029/jb095ib04p04943

Bohrmann, G., Chin, C., Petersen, S., Sahling, H., Schwarz-Schampera, U., Greinert, J., et al. (1998). Hydrothermal activity at Hook Ridge in the central Bransfield Basin, Antarctica. *Geo-Marine Letters*, *18*(4), 277–284. https://doi.org/10.1007/s003670050080

Bourouis, S., & Bernard, P. (2007). Evidence for coupled seismic and aseismic fault slip during water injection in the geothermal site of Soultz (France), and implications for seismogenic transients. *Geophysical Journal International*, *169*(2), 723–732. https://doi.org/10.1111/j.1365-246x.2006.03325.x

Buck, W. R. (2004). 1. Consequences of asthenospheric variability on continental rifting. In *Rheology and deformation of the lithosphere at continental margins* (pp. 1–30). Columbia University Press. https://doi.org/10.7312/karn12738-002

Cabrera, L., Poli, P., & Frank, W. B. (2020). A clustered preparatory phase of the 2009 Mw 6.3 L'Aquila earthquake. *AGU Fall Meeting Abstracts*, *2020*, S029.

Duverger, C., Lambotte, S., Bernard, P., Lyon-Caen, H., Deschamps, A., & Nercessian, A. (2018). Dynamics of microseismicity and its relationship with the active structures in the western Corinth Rift (Greece). *Geophysical Journal International*, *215*(1), 196–221. https://doi.org/10.1093/gji/ggy264

Dziak, R. P., Park, M., Lee, W. S., Matsumoto, H., Bohnenstiehl, D. R., Haxel, J. H., et al. (2010). Tectonomagmatic activity and ice dynamics in the Bransfield Strait back-arc basin, Antarctica. *Journal of Geophysical Research*, *115*(B1). https://doi.org/10.1029/2009jb006295

Farrell, J., Husen, S., & Smith, R. B. (2009). Earthquake swarm and b-value characterization of the Yellowstone volcano-tectonic system. *Journal of Volcanology and Geothermal Research*, *188*(1–3), 260–276. https://doi.org/10.1016/j.jvolgeores.2009.08.008

Frohlich, C., & Davis, S. (1993). Teleseismic b values; or, much ado about 1.0. *Journal of Geophysical Research*, *98*(B1), 631–644. https://doi.org/10.1029/92jb01891

Gibbons, S. J., & Ringdal, F. (2006). The detection of low magnitude seismic events using array-based waveform correlation. *Geophysical Journal International*, *165*(1), 149–166. https://doi.org/10.1111/j.1365-246x.2006.02865.x

Gràcia, E., Canals, M., Lí Farràn, M., José Prieto, M., & Sorribas, J., & Gebra Team. (1996). Morphostructure and evolution of the central and eastern Bransfield basins (NW Antarctic Peninsula). *Marine Geophysical Researches*, *18*(2–4), 429–448.

Gutenberg, B., & Richter, C. (1941). *Seismicity of the Earth* (Vol. 34). Geological Society of America.

Hainzl, S., Scherbaum, F., & Beauval, C. (2006). Estimating background activity based on interevent-time distribution. *Bulletin of the Seismological Society of America*, *96*(1), 313–320. https://doi.org/10.1785/0120050053

Heimisson, E. R., & Segall, P. (2020). Physically consistent modeling of Dike-induced deformation and seismicity: Application to the 2014 Bárðarbunga Dike, Iceland. *Journal of Geophysical Research: Solid Earth*, *125*(2), e2019JB018141. https://doi.org/10.1029/2019jb018141

Hill, D. P. (1977). A model for earthquake swarms. *Journal of Geophysical Research*, *82*(8), 1347–1352. https://doi.org/10.1029/jb082i008p01347

International Seismological Centre. (2021). *On-line bulletin*. https://doi.org/10.31905/D808B830

Istituto Nazionale di Oceanografia e di Geofisica Sperimentale. (1992). *Antarctic seismographic Argentinean Italian network—OGS*. International Federation of Digital Seismograph Networks.

Kato, A., Fukuda, J., Kumazawa, T., & Nakagawa, S. (2016). Accelerated nucleation of the 2014 Iquique, Chile Mw 8.2 earthquake. *Scientific Reports*, *6*(1), 1–9. https://doi.org/10.1038/srep24792

Mogi, K. (1962). Magnitude–frequency relation for elastic shocks accompanying fractures of various materials and some related problems in earthquakes. *Bulletin of the Earthquake Research Institute, University of Tokyo*, *40*, 831–853.

Mogi, K. (1963). Some discussions on aftershocks, foreshocks and earthquake swarms: The fracture of a semi-infinite body caused by an inner stress origin and its relation to the earthquake phenomena (third paper). *Bulletin of the Earthquake Research Institute, University of Tokyo*, *41*(3), 615–658.

Olivet, J. L., Sánchez Bettucci, L., Castro-Artola, O. A., Castro, H., Rodríguez, M., & Latorres, E. (2021). A seismic swarm at the Bransfield Rift, Antarctica. *Journal of South American Earth Sciences*, *111*, 103412. https://doi.org/10.1016/j.jsames.2021.103412

Omori, F. (1894). On the aftershocks of earthquake. *Journal of the College of Science, Imperial University of Tokyo*, *7*, 111–200.

Perfettini, H., & Avouac, J.-P. (2004). Postseismic relaxation driven by brittle creep: A possible mechanism to reconcile geodetic measurements and the decay rate of aftershocks, application to the Chi-Chi earthquake, Taiwan. *Journal of Geophysical Research*, *109*(B2). https://doi.org/10.1029/2003jb002488

Poli, P. (2017). Creep and slip: Seismic precursors to the Nuugaatsiaq landslide (Greenland). *Geophysical Research Letters*, *44*(17), 8832–8836. https://doi.org/10.1002/2017gl075039

Reiss, M. C., Muirhead, J. D., Laizer, A. S., Link, F., Kazimoto, E. O., Ebinger, C. J., & Rümpker, G. (2021). The impact of complex volcanic plumbing on the nature of seismicity in the developing magmatic natron rift, Tanzania. *Frontiers of Earth Science*, *8*, 609805. https://doi.org/10.3389/feart.2020.609805

Roberts, N. S., Bell, A. F., & Main, I. G. (2015). Are volcanic seismic b-values high, and if so when? *Journal of Volcanology and Geothermal Research*, *308*, 127–141. https://doi.org/10.1016/j.jvolgeores.2015.10.021

Roman, D. C., & Cashman, K. V. (2006). The origin of volcano-tectonic earthquake swarms. *Geology*, *34*(6), 457–460. https://doi.org/10.1130/g22269.1

Sánchez-Reyes, H., Essing, D., Beaucé, E., & Poli, P. (2021). The imbricated foreshock and aftershock activities of the Balsorano (Italy) M w 4.4 normal fault earthquake and implications for earthquake initiation. *Seismological Society of America*, *92*(3), 1926–1936.

Schorlemmer, D., Wiemer, S., & Wyss, M. (2005). Variations in earthquake-size distribution across different stress regimes. *Nature*, *437*, 539–542. https://doi.org/10.1038/nature04094

Sibson, R. H. (2000). Fluid involvement in normal faulting. *Journal of Geodynamics*, *29*(3–5), 469–499. https://doi.org/10.1016/s0264-3707(99)00042-3

Taylor, F. W., Bevis, M. G., Dalziel, I. W. D., Smalley, R., Frohlich, C., Kendrick, E., et al. (2008). Kinematics and segmentation of the South Shetland islands-Bransfield Basin system, northern Antarctic Peninsula. *Geochemistry, Geophysics, Geosystems*, *9*(4).

U.S. Geological Survey. (2020). *Earthquake Lists, maps, and statistics*. Retrieved from https://www.usgs.gov/natural-hazards/earthquake-hazards/lists-maps-and-statistics

Van der Elst, N. J., Savage, H. M., Keranen, K. M., & Abers, G. A. (2013). Enhanced remote earthquake triggering at fluid-injection sites in the midwestern United States. *Science*, *341*(6142), 164–167. https://doi.org/10.1126/science.1238948

Wiemer, S. (2001). A software package to analyze seismicity: ZMAP. *Seismological Research Letters*, *72*(3), 373–382. https://doi.org/10.1785/gssrl.72.3.373

Wilks, M., Kendall, J.-M., Nowacki, A., Biggs, J., Wookey, J., Birhanu, Y., et al. (2017). Seismicity associated with magmatism, faulting and hydrothermal circulation at Aluto Volcano, Main Ethiopian Rift. *Journal of Volcanology and Geothermal Research*, *340*, 52–67. https://doi.org/10.1016/j.jvolgeores.2017.04.003